

RSC Advances



This is an *Accepted Manuscript*, which has been through the Royal Society of Chemistry peer review process and has been accepted for publication.

Accepted Manuscripts are published online shortly after acceptance, before technical editing, formatting and proof reading. Using this free service, authors can make their results available to the community, in citable form, before we publish the edited article. This *Accepted Manuscript* will be replaced by the edited, formatted and paginated article as soon as this is available.

You can find more information about *Accepted Manuscripts* in the [Information for Authors](#).

Please note that technical editing may introduce minor changes to the text and/or graphics, which may alter content. The journal's standard [Terms & Conditions](#) and the [Ethical guidelines](#) still apply. In no event shall the Royal Society of Chemistry be held responsible for any errors or omissions in this *Accepted Manuscript* or any consequences arising from the use of any information it contains.

Synthesis of Gold Nanoparticles within Silica Monoliths through Irradiation Techniques using Au(I) and Au(III) Precursors

Matteo Tonelli^{†‡*}, Sylvia Turrell[‡], Odile Cristini-Robbe[†], Hicham El Hamzaoui[†], Bruno Capoen^{†*}, Mohamed Bouazaoui[†], Massimo Gazzano[♦], Maria Cristina Cassani[◇]

[†]PhLAM (CNRS, UMR 8523) and CERLA, Université Lille 1, Sciences et Technologies 59655 Villeneuve d'Ascq, France

[‡]LASIR (CNRS, UMR 8516) and CERLA, Université Lille 1, Sciences et Technologies 59655 Villeneuve d'Ascq, France

[♦]ISOF-CNR, c/o Dipartimento di Chimica "G. Ciamician", Università degli Studi di Bologna, Via Selmi 2, I-40126 Bologna, Italy

[◇]Dipartimento di Chimica Industriale "Toso Montanari", Università degli Studi di Bologna, Viale Risorgimento 4, I-40136 Bologna, Italy

[°]Present adress: Institut de Recherches sur la Catalyse et l'Environnement de Lyon, IRCELYON, UMR5256 CNRS-Université Claude Bernard Lyon 1, 2 avenue A. Einstein, F-69626 Villeurbanne cedex, France

Abstract

The formation of gold nanoparticles (GNPs) within mesoporous silica matrices by means of irradiation techniques is reported. The xerogels were impregnated with solutions of two different gold precursors: $(\text{Ph}_3\text{P})\text{AuCl}$ for Au(I) and $[\text{nBu}_4\text{N}]\text{AuCl}_4$ for Au(III). The irradiations were performed with two continuous wave laser sources (266 and 532 nm), with a femtosecond pulsed laser (800 nm), and with a mercury vapour lamp emitting in the UV region. It has been shown that no reducing agent was ever required to obtain GNP formation. XRD data exhibited the typical patterns of fcc gold, except for two cases involving the Au(I)-doped matrices, where a preferential crystallographic orientation was observed. Excluding the case of the UV irradiations performed on Au(III)-doped samples, we always obtained the formation of roughly spherical and well dispersed GNPs of relatively small size (6-60 nm). The gold-reduction mechanisms proposed depend on the chosen irradiation technique. Moreover, when laser sources are employed, GNP formation can be selectively limited to the irradiated areas, thus making it possible to obtain reproducible patterns of GNPs.

1. Introduction

The interest of the scientific community in gold nanoparticles (GNPs) has grown steadily over the last three decades, because of applications in numerous fields such as catalysis,¹ bio-sensing,² optics^{3,4} and medicine.⁵ Many fascinating possibilities are related to the Localized Surface Plasmon resonance (LSPR), which gives rise first to intense and tuneable extinction bands in the visible or NIR,⁶ and secondly to a dramatic increase in signals obtained from near-by molecules using Raman, infrared, and fluorescence spectroscopies.⁷⁻⁹

When embedded in transparent solid matrices, the nonlinear optical properties of GNPs make them attractive for optical telecommunications, computing and information processing.¹⁰⁻¹³ Even though a large number of synthetic routes have been developed to obtain dispersed GNPs in the liquid phase with controlled sizes and shapes, their inclusion in solid host matrices is not at all a trivial task. One possible approach to obtain GNP-composite materials is the straightforward reaction in the liquid phase between a properly chosen gold precursor and a chemically active support.^{14,15} A second possibility is to soak a porous material in the gold precursor and obtain GNP formation in a subsequent step by means of chemical reduction^{16,17} or photochemical methods.¹⁸

Space-localization of nanocrystals formation in silica matrices is desirable for certain applications such as tuneable optical filters.¹⁹ In effect, it is a tailor-made fashion of inducing localized refractive index changes *via* the optical nonlinearities of the GNPs. Such localized particle growth can be attained by using laser irradiation with the adapted precursors in the matrix.

Concerning this laser-irradiation technique, most of the previous studies have employed Au(III) precursors^{14,20} and in particular tetrachloroauric acid.^{15-17,21,22} For example, we have recently reported that femtosecond laser irradiation of mesoporous silica matrices doped with H₂AuCl₄ gives rise to the formation of GNPs, but only in the presence of a reducing agent.²² However, the presence of these chemical species can be detrimental to the optical properties of the final material.

The main objective of the present study was to find conditions for a simple, straightforward method to generate stable localized nanoparticles without the need of additives, even in a

femtosecond irradiation regime. As irradiation techniques allow a spatial control of GNP growth, four different irradiation sources were used (lasers emitting at 266, 532 and 800 nm and a UV lamp) to irradiate silicate matrices doped with either Au(I) or Au(III) precursors. Finally, a more fundamental aim was to elucidate the gold reduction mechanisms that allow the formation of the GNPs and also to study the influence of the two precursors on the structural properties of the particles.

2. Experimental

2.1 Sample preparation

Matrices. Monolithic mesoporous silica hosts were prepared *via* a base-catalysed sol-gel route at 50°C and then calcined at 850°C as previously described.²³ Isothermal nitrogen sorption measurements, interpreted using the BJH model, showed that these silica xerogels possess an average pore-size distribution of 5.5 nm, a specific surface area of 360 m²g⁻¹ and a total pore volume of 0.49 cm³ g⁻¹. The nitrogen adsorption-desorption isotherm profiles are consistent with cylindrically-shaped pores, with a random space-distribution and a certain pore interconnectivity. These properties are important, as the small pores can prevent nanoparticle-clustering and interconnecting pores favour distribution of dopant species. Finally, a high surface area can be advantageous in the case of catalytic applications.

Gold precursors. The preparation of triphenylphosphine gold chloride (Ph₃P)AuCl, and tetrabutylammonium tetrachloroaurate [nBu₄N]AuCl₄, followed published procedures²⁴⁻²⁶ (see Supporting Information).

Impregnation of silica matrices. The mesoporous silica hosts were immersed for 4 hours at room temperature in a 0.02 M dichloromethane (DCM) solution of the chosen gold precursor. All impregnations were carried out in the dark. The samples were then dried in an oven at 50°C.

2.2 Irradiation techniques

Femtosecond irradiations were carried out using a Ti: sapphire oscillator, coupled with a regenerative amplifier producing 120 fs pulses at $\lambda = 800$ nm at a 1 kHz repetition rate. The resulting spot, with an estimated size of 2 μm , was obtained by focusing the beam within the silica matrix using a $\times 10$ microscope objective (numerical aperture NA = 0.25). The samples impregnated with the Au(I) precursor were irradiated at the following beam powers (measured at the exit of the objective): 60, 30 and 20 mW. As the Au(III) precursor is a less stable species, the samples impregnated with this compound were irradiated at 30, 15 and 10 mW. The irradiations at 532 nm were performed with the beam of a doubled Nd:YAG laser, focused with a $\times 50$ Long Working Distance microscope objective (NA = 0.5). The laser-beam diameter was estimated to be 0.9 μm and the beam power impinging on the sample was 48 mW. This setup was coupled with a Raman spectrometer. Laser irradiations in the UV region were performed with a continuous wave (CW) solid state laser operating at $\lambda = 266$ nm. A $\times 80$ microscope objective with a numerical aperture of 0.55 was used to focus the beam on the samples. The spot diameter was estimated to be 1.7 μm and the power of the beam was 9.6 mW. In all cases of laser irradiation, the sample was fixed on a platform with micro XYZ adjustments, making it possible to create reproducible microarrays of GNPs within the sample. The UV lamp irradiations were performed with a high-pressure, quartz-sheathed mercury vapour lamp (Helios Italquartz UV12F). The lamp functioned at 125 W and was equipped with a water-cooling system. The emission spectrum of the lamp provided by the manufacturer shows that several emission lines are present in the UV region, the most intense of which fall at about 315 and 365 nm. The samples were fixed on the water-cooled jacket, between the cathode and the anode of the UV lamp, where the most intense radiation was expected. The irradiations lasted 10 minutes.

2.3 Sample washing and subsequent heat-treatments

After irradiation, the porous nature of these matrices made it possible to evacuate the non-reduced precursor by redissolving it in a fresh solvent. For thermal stability studies, some of the irradiated samples were placed overnight in DCM in a Soxhlet extractor. No cracking or loss of transparency

of the matrices was observed after washing. Once the residual precursors were evacuated from the silica host, the stability of the irradiation-induced GNPs was studied *via* subsequent heat-treatments. For this procedure, a heating rate of 200°C/h was used and the samples were maintained for one hour at a temperature between 200 and 600°C.

2.4 Characterization of the samples

Optical absorption spectra were recorded at room temperature using a Perkin-Elmer Lambda 19 UV-vis-IR double-beam spectrometer. X-ray diffraction (XRD) patterns were collected with Cu K α radiation by means of an X'Pert PANalytical diffractometer equipped with a fast X'Celerator detector. Data collections were carried out counting 500 s each 0.066° (2 θ) for diagnostic purposes and counting 3000 s each 0.033° (2 θ) to perform crystal-size (CS) measurements. The line broadening of the (111) reflections was used to evaluate the width of the crystal domains (τ_{111}) along the diagonal of the gold fcc cell. The values of τ_{111} were calculated from the FWHM (β) using the Scherrer equation.²⁷ TEM images were taken with a Philips CM30 microscope operating at 300 kV. In the case of the presence of nanoparticles, the irradiated surface was scratched and the resulting powder was ground in order to obtain a sufficiently small grain size. This fine powder was first deposited on a 200 mesh copper grid covered with a thin carbon membrane, and then metalized with a vaporized carbon layer. Raman micro-spectroscopy measurements were collected using a Horiba Jobin Yvon LabRam HR spectrometer operating at $\lambda = 532$ nm.

3. Results and discussion

3.1 Light-induced formation of GNPs

The results obtained with irradiations of samples containing the Au(I) and Au(III) precursors are summarized in Table 1.

Table 1 Effect of various irradiations of gels loaded with Au(III) and Au(I) precursors

Irradiation	LSPR wavelength (nm)		XRD average CS (nm)		Advantages
	Au (I)	Au (III)	Au (I)	Au (III)	
UV lamp	520	Blackening of the surface	7.5	24	Fast, Low cost
266 nm	530	Blackening of the surface	27	22	2D GNPs arrays possible. High spatial resolution
532 nm	538	532	14	20	2D GNPs arrays possible. Widespread equipment
800 nm	517	530	30	14	3D GNPs arrays possible. Not limited to transparent materials

For both precursors, gold reduction was always observed, regardless of the type of irradiation employed. The ruby-red colour characteristic of small GNPs was always detected after irradiation, except in the cases of the Au(III)-doped samples which blackened on the surface when exposed to UV light. The darkening of the surface could arise from the formation of relatively large GNP aggregates, which are known to cause a broadening and a red-shift of the LSPR band.²⁸ As a consequence, for these samples, the LSPR peak position could not be determined as the very strong light absorption by the irradiated area led to saturation of the detector. In all other cases, the UV-visible absorption spectra showed a single LSPR absorption band centred between 517 and 538 nm. These spectra are characteristic of relatively small (diameters < 50 nm), non-aggregated spherical GNPs dispersed in a silicate dielectric medium.^{29,30} Important to note is that in no case was the addition of a reducing agent required to obtain GNP formation. In Fig. 1, which presents results obtained with the Au(I) precursor, it is possible to observe that when UV irradiation is used, the absorbance of the LSPR band is lower than in the cases of irradiations at 532 or 800 nm. This weak absorbance level is due to the fact that the matrix itself is a strong absorber at short wavelengths and thus GNPs are formed only in the first few μm of the surface. Very similar results were obtained for samples doped with the Au(III) precursor.

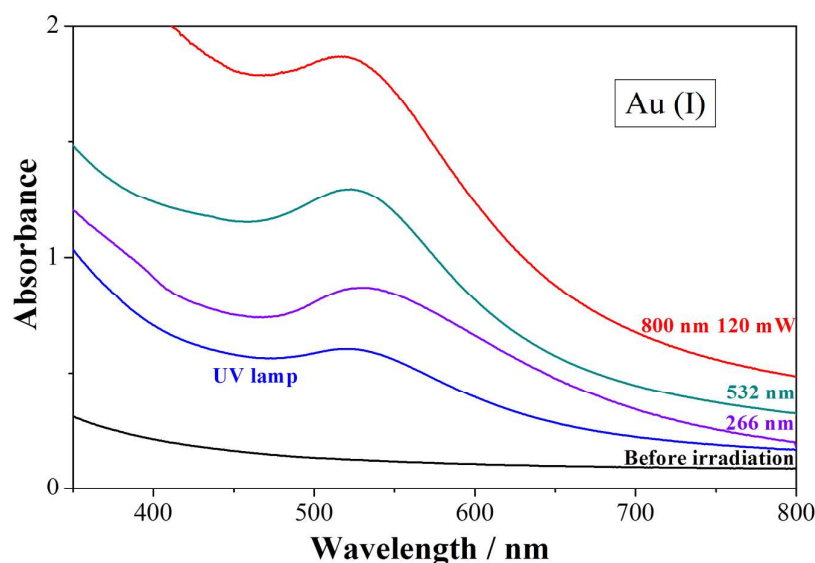


Fig. 1 Absorption spectra of the Au(I)-doped samples before and after irradiation with different light sources.

3.2 Structural and morphological study of GNPs

In all samples, the XRD patterns exhibited reflections typical of crystalline fcc gold, with intensity ratios of the reflections characteristic of a random distribution of the crystal domains. However, in the case of the Au(I)-doped samples irradiated at 266 and 800 nm, the (111) reflection was much stronger than the others, suggesting that the GNPs were formed with a preferential crystallographic orientation. An example is shown in Fig. 2, where a comparison is made of the characteristic XRD patterns obtained for Au(III)- and Au(I)-doped samples irradiated with a femtosecond laser at 800 nm. The respective normalized intensities of (111), (200), (220), (311) reflections, which are 1, 1/2, 1/3, 1/3 for the Au(III)-doped sample, become about 2.3, 1/2, 1/3, 1/3 for the Au(I)-doped one. These results suggest the presence of an excess of (111) planes oriented parallel to the measuring plane, *i.e.* the main plane of the sample (see sketch 1 in SI). To confirm this hypothesis, a portion of the GNP layer of a Au(I)-doped sample irradiated with a femtosecond laser at 800 nm, was manually detached from the matrix with a silica-glass tool (so as to avoid contamination) and

ground. The peak intensities observed in the resulting XRD pattern indicate that grinding removes the preferential (111) plane orientation caused by the femtosecond irradiation.

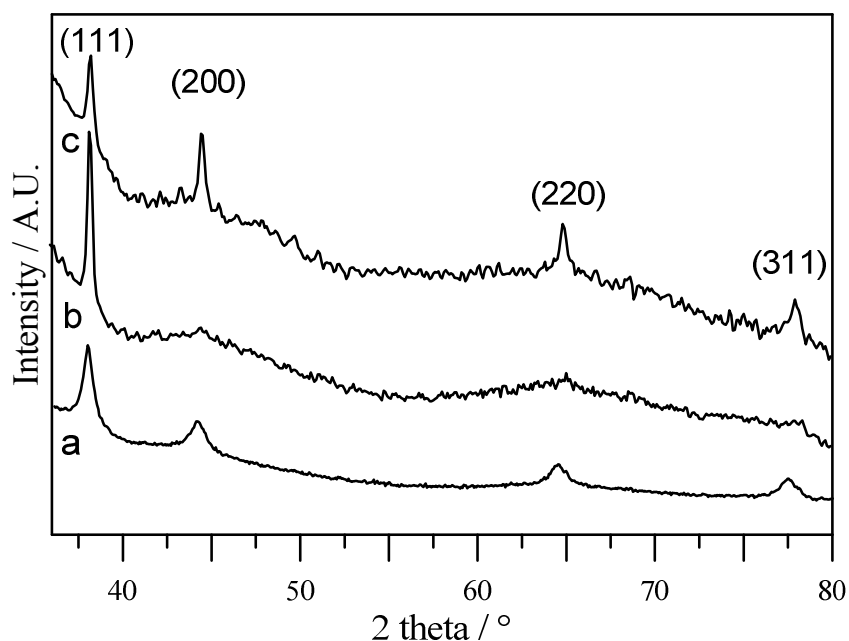


Fig. 2 XRD patterns of a) Au(III), b) and c) Au(I) doped samples after irradiation with a femtosecond 800 nm laser. The pattern c) is obtained from a removed portion of the matrix containing the GNP layer, which was ground manually.

This interpretation was confirmed by repeating the femtosecond experiment using three different laser powers. With the Au(I)-doped samples, irradiations at 20, 30 and 60 mW all yielded peaks of the (111) reflections which were much stronger in intensity and narrower in width than the reflections from the other planes (See Fig. 1S). On the other hand, irradiation of the Au(III)-doped samples with the three beam powers (10, 15 and 30 mW) never showed GNPs growing with a preferential crystallographic orientation.

Preferred orientation has been reported for GNPs formed on an organic monolayer or within Au-containing membranes *via* other synthetic procedures.^{14,31-34} In one case, the (111) preferred

growth of GNPs was observed in mesoporous silica films³⁵ after H₂-reduction of Au³⁺ ions. These authors suggested that the anisotropic orientation of the Au nanoparticles resulted from the formation of arrays of several Au domains located along oriented mesopores. However, in our work, no such organization linking crystal domains could be detected in TEM images and the pore channels of bulk xerogels where the GNPs have been precipitated are randomly distributed. Hence, our experimental data suggest a growth in the preferred direction perpendicular to (111) planes, possibly due to a photo-chemical reduction of the Au(I) precursor, as will be discussed in section 3.3. To the best of our knowledge, the present work is the first in which preferred (111) orientation is obtained inside bulk inorganic matrices with non-structured pores.

The effect of the gold precursor and of the different kinds of irradiations on the size of the synthesized GNPs was investigated by means of XRD and TEM. An experimental estimation of the crystal or domain size in a direction perpendicular to a crystal plane (111) was obtained using the Scherrer equation and the width of the (111) peak.²⁷ This particular direction has been chosen for the CS calculation because it corresponds to the most intense reflection in the oriented samples, as explained above. Comparison of columns 4 and 5 of Table 1 shows that the kind of irradiation employed does not seem to produce a significant difference in the size of the GNPs obtained with the Au(III)-doped samples, for which the average size is almost always in the range 20 nm. However, for the Au(I)-doped samples, the GNP size varies from 7.5 nm when the nanoparticles are formed *via* 10 min exposure to a UV lamp, to 30 nm, about four times larger, when the samples are irradiated with the 800 nm pulsed laser at 20 mW.

Finally, the effect of the laser power affects the Au(I)- and the Au(III)-doped samples differently. While the Au(III)-doped samples irradiated with the 800 nm pulsed laser at 30, 15 and 10 mW showed virtually no variation in average GNP size, for the Au(I)-doped samples, an increase of the laser beam power resulted in an increase of the average CS (30, 34 and 37 nm for 20, 30 and 60 mW, respectively). These observations suggest that the use of the Au(I) precursor makes

it possible to adjust the size of the GNPs obtained, either by choosing the type of irradiation, or by varying the laser intensity.

TEM analyses revealed other differences between the two precursors. Fig. 3 presents images obtained for the Au(III)- and Au(I)-doped samples after irradiation with the 800 nm pulsed laser at 30 and 60 mW, respectively. For the Au(III)-doped samples, the imaging shows the presence of “spheroidal” gold nanocrystals with a relatively broad size distribution (6-60 nm). However, closer observations of some of the larger “particles” show some irregular shapes (see Fig. 3b), which were never found for the Au(I) precursor.

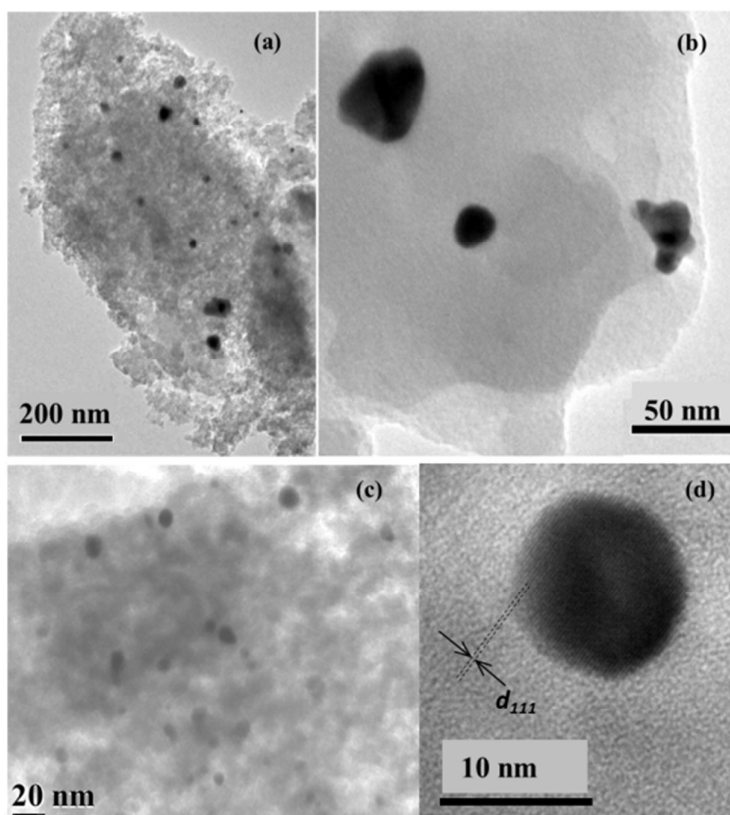


Fig. 3 a) TEM images of Au(III)-doped sample after femtosecond irradiation showing GNPs in the 6-60 nm size range. b) Enlarged view of the same Au(III)-doped sample showing irregular shaped GNPs. c) TEM image of the Au(I)-doped sample after femtosecond irradiation, showing GNPs of sizes inferior to 20 nm. d) Enlarged view of a nanoparticle showing (111) planes in the Au(I)-doped sample.

Fig. 3c shows some of the relatively small, spherically shaped GNPs obtained with the Au(I) precursor. In this case, there is a rather narrow size distribution and the particles are well dispersed in the matrix with no apparent aggregation. High resolution TEM images exhibit lattice planes of the gold structure (Fig. 3d). In the portion of the sample analysed by TEM, these particles are generally smaller than the estimates from XRD data. Fukuoka et al observed similar results with GNPs in hexagonal mesoporous silica films.³⁵

3.3 Gold reduction mechanism

The irradiations performed with the UV lamp on the Au(III)- and Au(I)-doped samples led to very different results (Fig. 4). As reported in Table I and as can be seen from Figs. 4a and 5a, UV exposure of the sample doped with the yellow Au(III) precursor caused a darkening of the surface and a discoloration of the matrix under the darkened layer. The newly formed colourless layer started to disappear a few hours after the irradiation and turned totally black overnight (Fig. 5b). On the other hand, the UV lamp-irradiation on the initially colourless Au(I)-doped sample led to a pinkish coloration of the very first few μm of the surface (Fig. 4b), leaving the rest of the matrix unchanged.

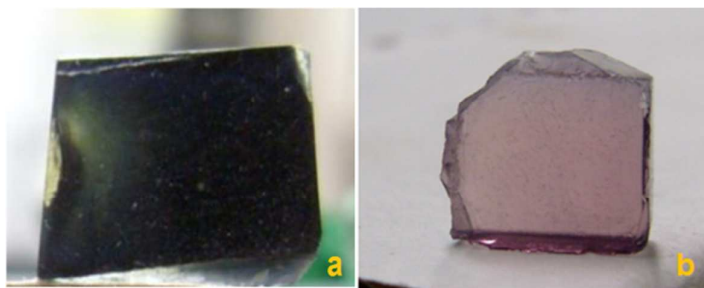


Fig. 4 Effect of UV lamp irradiation on a) Au(III)- and b) Au(I)-doped samples.

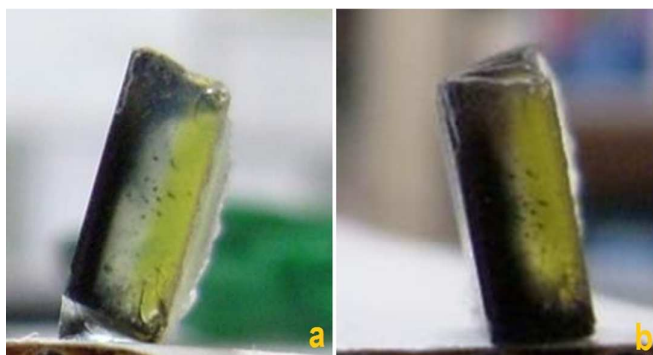


Fig. 5 Au(III)-doped sample: a) immediately after UV irradiation b) 24 hours after UV irradiation.

The local discoloration of the Au(III)-doped sample was investigated by irradiating a freshly prepared sample with the unfocused beam of a CW laser operating at 351 nm, which is energetically close to the most intense emission line of the UV mercury vapour lamp. As it can be seen from the results in Fig. 6, a significant reduction of the absorbance around 320 nm and in the visible region was observed 10 minutes after the irradiation. A band in this region can be ascribed to the Ligand-To-Metal Charge Transfer (LMCT) in the tetrachloroaurate ion.³⁶ This band is clearly observable at 321 nm in the spectra after irradiation and gradually increases in height with time, as a broad LSPR peak centered at about 660 nm appears, causing the darkening of the irradiated area.

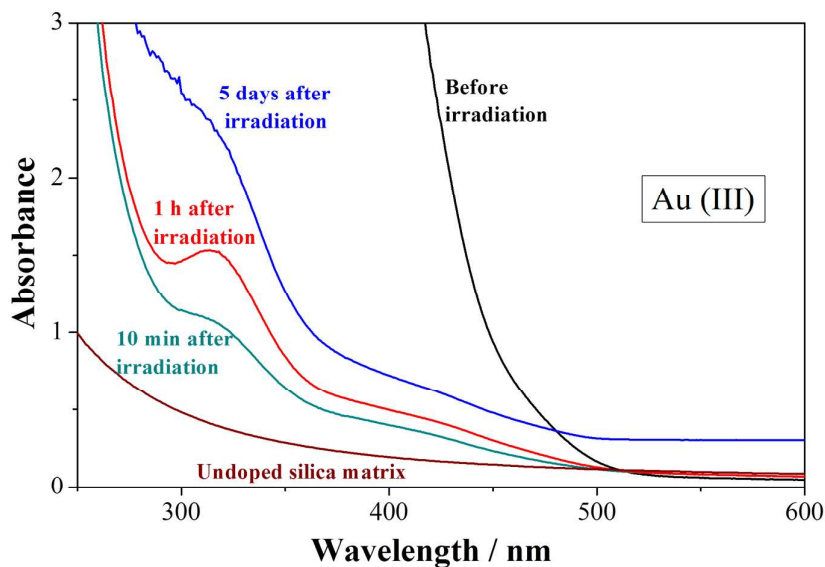


Fig. 6 Absorption spectral evolution of an Au(III)-doped sample irradiated at 351 nm.

These results can be explained by a mechanism of intracomplex photoreduction which was previously reported for HAuCl_4 solutions under UV irradiation.³⁷⁻³⁹ It is generally accepted that the first step is the absorption of UV radiation by the very broad LMCT band of the $[\text{AuCl}_4]^-$ ion, forming an excited charge transfer state. When the electron is completely detached from the chlorine, ion photodissociation occurs so that AuCl_3^- and chlorine radical are formed:



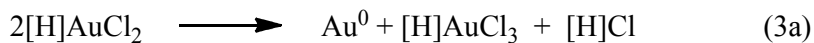
The Au(II) intermediate is very unstable and, according to DFT calculations, is reduced by disproportionation rather than by chlorine atom dissociation:⁴⁰



During UV irradiation, the change in colour occurs because the Au(I) intermediate does not absorb in the visible and near-UV regions.³⁹⁻⁴¹ At the same time, while $[\text{AuCl}_4]^-$ is consumed by reaction

(1), the matrix becomes more and more transparent to the radiation at 351 nm, causing the discoloration to proceed at deeper layers within the sample, as observable in Fig. 5a.

Once the irradiation is stopped, the disappearance in Fig. 5b of the colourless layer containing the Au^+ intermediate is explained as the product of a dismutation reaction occurring in two steps:³⁹



It should be noted that in our case, the hydrogen in the brackets of the equations above comes from one of the alkyl chains of the ligand. Eventually, the Au^0 which is formed aggregates into relatively large nanoparticles having a very broad LSPR absorption band, which causes the observed darkening of the surface. On the other hand, the appearance of AuCl_4^- explains the increase in intensity of the absorption band around 320 nm. A photochemical gold-reduction mechanism can be proposed also in the case of the UV irradiation of the Au(I)-doped samples. Indeed, GNPs were formed when the Au(I)-doped samples were irradiated at 266 nm but not at 351 nm. This observation can be explained by the fact that the LMCT band of $(\text{Ph}_3\text{P})\text{AuCl}$ falls below 280 nm (see Fig. 6S), and thus photolysis of the gold precursor cannot occur at 351 nm.

In the case of GNP formation under the irradiation at 532 nm, only a thermal reduction mechanism can be proposed, as neither $[\text{nBu}_4\text{N}]\text{AuCl}_4$ nor $(\text{Ph}_3\text{P})\text{AuCl}$ exhibit a LMCT band in the visible region (Figs. 6S and 7S). It should be noted that for both precursors, GNP formation occurred only when a definite laser-beam-power threshold was reached. The threshold power was estimated to be 4.8 mW and 48 mW for the Au(III)- and Au(I)-doped samples, respectively. For powers close to the threshold, gold reduction was observed only after a certain induction time, probably because time was required to reach the decomposition temperature of the precursors.

This phenomenon was investigated by recording Raman spectra during the irradiation. As can be seen from Figs. 7 and 9S, at the very beginning of the irradiation, the spectra were

characteristic of the non-irradiated doped matrices, with bands of the Au(I) precursor (999, 1028 and 1103 cm^{-1}) clearly recognizable on the background signal from the silica matrix. As soon as the GNPs started to form, an increase of the background signal was observed, due to fluorescence. At longer irradiation times, the bands of the precursor diminished in intensity while new spectral features started to grow at 1350 and 1590 cm^{-1} . These bands are attributed to the formation of amorphous carbon originating from the thermal decomposition of the precursors.⁴² The carbon is also the cause of the strong fluorescence background. Similar results were obtained for the Au(III)-doped samples. Hence, even though the local temperature increase was not measured, our data support hypothesis of a thermal reduction mechanism.

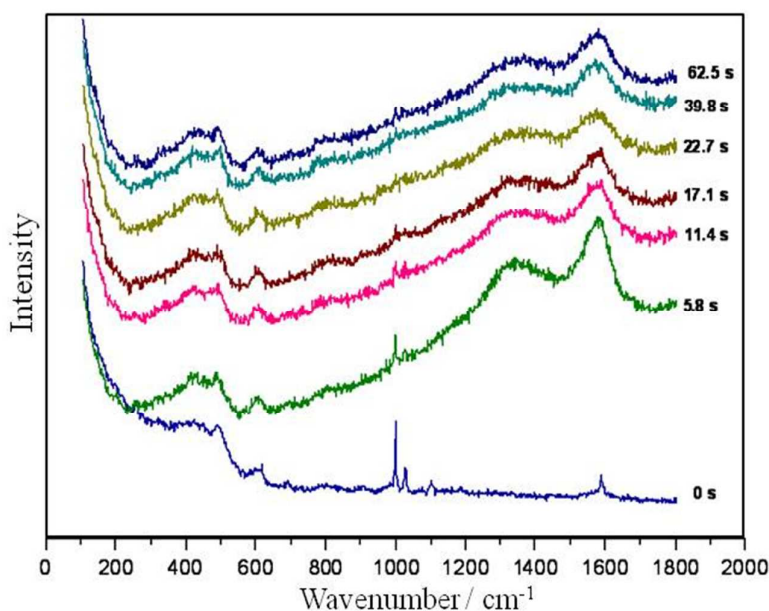


Fig. 7 Evolution of the Raman spectra collected at different time intervals for the Au(I)-doped sample (Laser power = 48 mW, $\lambda_{\text{exc}} = 532 \text{ nm}$).

Finally, in the case of the pulsed femtosecond irradiation at 800 nm, the gold reduction is likely to be mostly photo-chemical. In effect, even though there is no linear absorption from the matrix or from the precursors, the very high peak intensities generated by a femtosecond pulsed laser as that employed in our experiments can lead to multiphoton absorption phenomena.^{43,44} No simple experiment can inform us about the order of this nonlinearity, but such effects are able to

induce both thermal and photochemical gold reduction mechanisms, even though the latter is the most likely to occur. Indeed, while a significant instantaneous and localized increase of temperature cannot be excluded, due to multi-photon absorption in this ultra-short pulse regime, the low cadence of the laser limits the average heating effects, which can be evaluated at a few degrees.²²

Two-photon absorption is tantamount to one-photon absorption with the wavelength 400 nm, whereas three-photon absorption corresponds to the energy of a photon at 266 nm. Hence, the LMCT level can be excited by this way, leading to the photo-mechanisms previously exposed. Moreover, some of our experimental results seem to corroborate this thesis. In this regard, it is interesting to note that for the Au(I)-doped samples, the results obtained with the pulsed laser at 800 nm are surprisingly similar to what is observed in the case of the irradiation at 266 nm: in both cases, XRD patterns revealed a much stronger intensity of the (111) reflection (see Figs. 2, 1S and 2S) and similar values of the average CS. When the GNPs were grown by the thermal decomposition of the precursor, caused by irradiation at 532 nm, no such preferential orientation was observed. Additionally, if the irradiations at 800 nm caused a reduction which was purely thermal, it should also be possible to obtain GNPs when the matrices are impregnated with HAuCl₄ alone. Our previously published results²² show that this is not the case, even if the temperature of decomposition of HAuCl₄ in air (170°C)⁴⁵ is lower than that of either [nBu₄N]AuCl₄ or (Ph₃P)AuCl (see Figs. 11S and 12S).

3.4 Localized formation of stable GNPs

A major difference between the irradiation performed with the UV lamp and the laser sources lies in the ability to grow the GNPs in selected areas of the sample. Fig. 8 shows an example of the microarrays of GNPs easily obtainable within the silica matrix when a laser source of irradiation is employed. The spacing of the obtained lines and their final pattern can be changed without difficulty, as the focused beam acts like the tip of a pencil causing GNP formation only in the irradiated areas. As indicated in the last column of Table I, the irradiation at 266 nm made it

possible to achieve the highest resolution in the micropatterning of the GNPs. This fact was due to two phenomena: on one hand, due to minimal diffraction, smaller beam spots can be obtained at this wavelength; on the other hand, the formation of GNPs outside of the irradiated area was minimized probably because of the photochemical nature of the reduction mechanism.

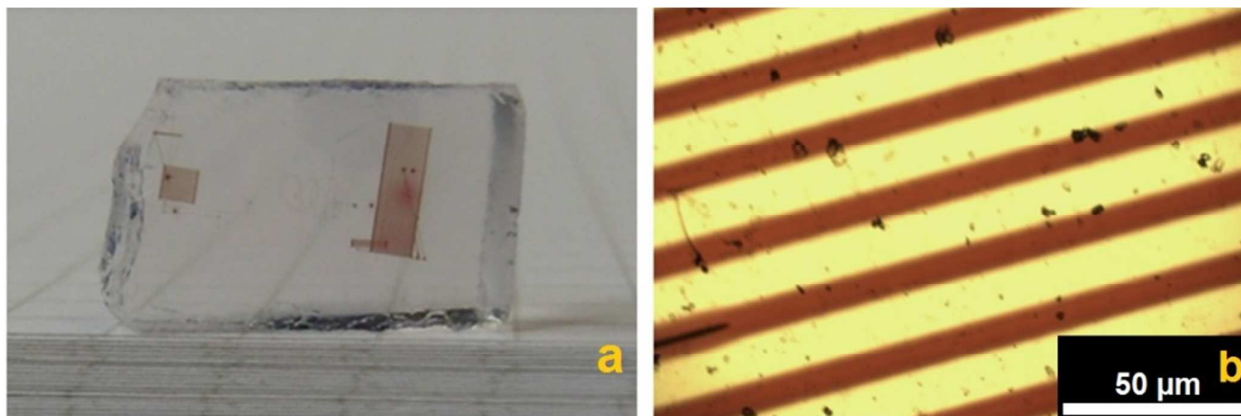


Fig. 8. a) Au(I)-doped sample after irradiation with CW laser operating at 266 nm. b) close-up of a).

Looking again at the last column of Table I, another difference among the various irradiation techniques is noted. When pulsed radiation at 800 nm is employed, the formation of GNPs is not limited to the sample surface, but can also be induced in the bulk of the matrix. It is thus possible with this technique, to grow GNPs selectively in 3D micro-patterns. Such a result was not obtained for the irradiations at 266 or 532 nm, as in these cases the GNP formation was limited to the surface of the matrix. Obviously, in the case of 266 nm irradiation, limitations arise from the strong absorption displayed by the silica matrix and the gold precursor in this spectral region. However, when irradiation at 532 nm is used, there is almost no absorption by the matrix. Hence, the difficulty of penetrating must be due to scattering effects. Indeed, as light scattering processes essentially vary with $1/\lambda^4$, the laser beam at 800 nm would converge to the focal point better than an excitation at 532 nm.

From an applicative point of view, the formation of GNPs, as well as their 2D and 3D microarrays would be of little or no use if it were not possible to remove the gold precursors from the host matrix. Indeed, the precursors within the porous silica samples are not thermally stable, and their reduction at room temperature was observed in non-irradiated samples kept in the dark for 6 months. In this work, the precursors were eliminated by immersing the irradiated samples in a fresh solvent solution. This process efficiently removes most of the precursor, as attested by the absence of any further colouration after annealing. It was found that the resulting matrices can be re-impregnated with a different solution. Hence, this technique provides a method to obtain a GNP-containing mesoporous material, which can be employed as a host for further doping or deposition processes.

Following the washing procedure, the thermal resistance of the deposited GNP microarrays was tested. It was found that the GNP microarrays remained stable even at 600°C, with no sign of GNP diffusion outside of the irradiated areas. As seen from the results in Fig. 9, a blue-shift and a narrowing of the LSPR band is observed with increasing annealing temperatures for the Au(III)-doped sample (Similar results were observed with the Au(I) precursor). Two hypotheses can be advanced to explain this phenomenon: a reshaping of the GNPs or a change in the contact between the pores and the nanoparticle surfaces.

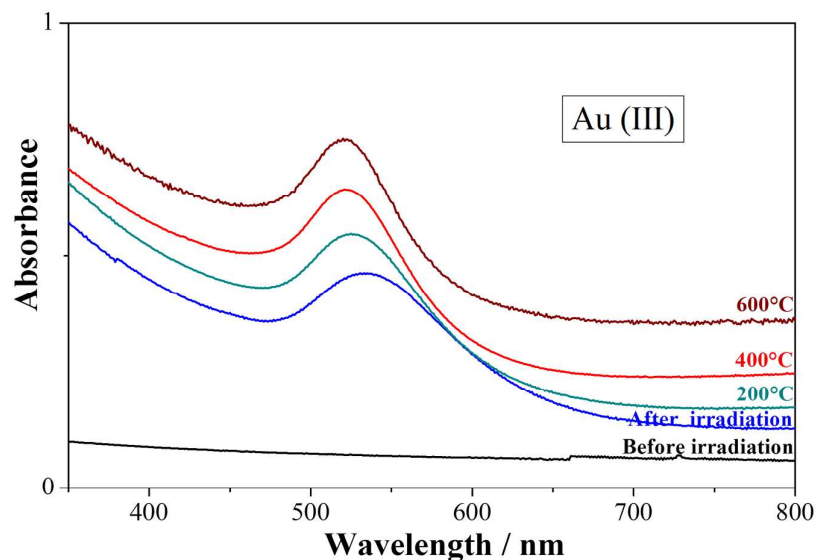


Fig. 9. Thermal variations of the absorption spectra of the sample impregnated with the Au(III) precursor and irradiated at 532 nm.

For the first case, it is known that annealing leads to a thermally driven process that causes GNPs to become more spherical and to increase the distance between them. Hence, this effect leads to a more uniform distribution of the GNP size and consequently to a narrowing of the LSPR absorption band. The increased inter-particle separation is supposed to be the origin of the observed blue-shift in the absorption band.^{46,47} Secondly, it cannot be excluded that a concomitant rearrangement of the silica matrix can occur during the annealing process. The consequent change in the pore-nanoparticle surface contact would cause a change in the value of the dielectric constant surrounding the GNPs, thus contributing further to an observed blue shift.

From these results, it is seen that a simple control of the annealing temperature makes it possible to tailor the position of the LSPR band of synthesized GNPs. This tailoring allows a fine tuning of the plasmonic effects, an aspect which could be useful for applications like biological sensors.

4. Conclusions

We have shown that GNPs can be easily obtained within mesoporous silica matrices using light-irradiation techniques. Our approach to form nanocrystals may share some similarities with recent research on Metal-Organic Frameworks (MOFs) where metallic or semiconducting nanoparticles could be created under the electron beam of a microscope, depending on the composition and structure of the surrounding matrix⁴⁸. Whereas the e-beam technique is well-suited for nanoscale high-resolution writing of very small nanoparticles in a porous medium, the laser-irradiation method is devoted to the micron-scale localisation of various kinds of nanoparticles in largely exposed areas. One advantage of the precursors investigated in this study is that no reducing agent is required to form GNPs. The Au(I) precursor yields small and non-aggregated GNPs, even with the irradiation of a simple UV lamp, thus making this photosynthetic route a possible fast and low-cost method to obtain well dispersed GNPs. It seems that the use of Au(I) precursor can also be preferred to control the particle size distribution. Laser irradiation techniques provide the additional advantage of forming GNPs only in chosen irradiated areas. Consequently, very stable and reproducible micropatterns of GNPs can be designed within such matrices. We have proposed two mechanisms for gold reduction which depend on the irradiation technique used. Accordingly, the process is predominantly photochemical under UV or fs pulsed radiation but is mainly thermal in the case of laser excitation at 532 nm.

The porous nature of the matrices made it possible to remove the unreacted precursors after irradiation. A simple washing procedure stabilizes the samples by preventing any further gold reduction. Thus, these GNP porters are potentially attractive in a number of applications, such as catalysis and sensoristics, as they can be re-impregnated repeatedly. Finally, annealing tests of the washed GNP-containing matrices proved that for temperatures up to 600°C, almost no aggregation or diffusion of GNPs occurs outside of the irradiated areas.

Acknowledgments

This work was supported by the Nord-Pas de Calais Regional Council and FEDER through the ‘Contrat de Projets État Région (CPER) 2007–2013’ and the ‘Campus Intelligence Ambiante’ (CIA). M.C.C. wishes to thank the University of Bologna and the Ministero dell’Università e della Ricerca (MUR) (project: “New strategies for the control of reactions: interactions of molecular fragments with metallic sites in unconventional species”, PRIN 2009) for financial support. O. C. and M.C.C. wish to thank the Università Italo Francese (Galileo 2012, G12-212) for financial support.

References

- 1 C. Della Pina, E. Falletta, L. Prati and M. Rossi, *Chem. Soc. Rev.*, 2008, **37**, 2077–2095.
- 2 S. Song, Y. Qin, Y. He, Q. Huang, C. Fan and H.-Y. Chen, *Chem. Soc. Rev.*, 2010, **39**, 4234–4243.
- 3 M. K. Hossain, Y. Kitahama, G. G. Huang, X. Han and Y. Ozaki, *Anal. Bioanal. Chem.* 2009, **394**, 1747–1760.
- 4 A. L. Stepanov, *Rev. Adv. Mater. Sci.*, 2011, **27**, 115–145.
- 5 A. Llevot and D. Astruc, *Chem. Soc. Rev.*, 2012, **41**, 242–257.
- 6 K. L. Kelly, E. Coronado, L. L. Zhao and G. C. Schatz, *J. Phys. Chem. B*, 2003, **107**, 668–677.
- 7 N. P. W. Pieczonka and R. F. Aroca, *Chem. Soc. Rev.*, 2008, **37**, 946–954.
- 8 X. He, K. Wang and Z. Cheng, *Wiley Interdiscip. Rev. Nanomed. Nanobiotechnol.*, 2010, **2**, 349–366.
- 9 Y. Fu, J. Zhang and J. R. Lakowicz, *J. Am. Chem. Soc.* 2010, **132**, 5540–5541.

- 10 H. Inouye, K. Tanaka, I. Tanahashi, Y. Kondo and K. Hirao, *J. Phys. Soc. Jpn.*, 1999, **68**, 3810–3812.
- 11 D. Wan, H.-L. Chen, S.-C. Tseng, L. A. Wang and Y.-P. Chen, *Acs Nano*, 2010, **4**, 165–173.
- 12 A. Dhawan and J. F. Muth, *Nanotechnology*, 2006, **17**, 2504–2511.
- 13 X. Zhang, B. Sun, R. H. Friend, H. Guo, D. Nau and H. Giessen, *Nano Lett.*, 2006, **6**, 651–655.
- 14 B. Ballarin, M. C. Cassani, D. Tonelli, E. Boanini, S. Albonetti, M. Blosi and M. Gazzano, *J. Phys. Chem. C*, 2010, **114**, 9693–9701.
- 15 S. Fazzini, D. Nanni, B. Ballarin, M. C. Cassani, M. Giorgetti, C. Maccato, A. Trapananti, G. Aquilanti and S. I. Ahmed, *J. Phys. Chem. C*, 2012, **116**, 25434–25443.
- 16 Q. Lu, F. Cui, C. Dong, Z. Hua and J. Shi, *Opt. Mater.*, 2011, **33**, 1266–1271.
- 17 Y.-S. Chi, H.-P. Lin and C.-Y. Mou, *Appl. Catal. Gen.*, 2005, **284**, 199–206.
- 18 W. Chen, J.-Y. Zhang, Y. Di and I. W. Boyd, *Inorg. Chem. Commun.*, 2003, **6**, 950–952.
- 19 I. Riant and C. Belouet, (Alcatel) US20070183048 A1, 2007.
- 20 M. Behera and S. Ram, *Appl. Nanosci.*, 2013, **3**, 83–87.
- 21 H. El Hamzaoui, R. Bernard, A. Chahadih, F. Chassagneux, L. Bois, B. Capoen and M. Bouazaoui, *Mater. Res. Bull.*, 2011, **46**, 1530–1533.
- 22 H. El Hamzaoui, R. Bernard, A. Chahadih, F. Chassagneux, L. Bois, D. Jegouso, L. Hay, B. Capoen and M. Bouazaoui, *Mater. Lett.*, 2010, **64**, 1279–1282.
- 23 H. El Hamzaoui, L. Courthéoux, V. N. Nguyen, E. Berrier, A. Favre, L. Bigot, M. Bouazaoui and B. Capoen, *Mater. Chem. Phys.*, 2010, **121**, 83–88.
- 24 N. J. Destefano and J. L. Burmeister, *Inorg. Chem.*, 1971, **10**, 998–1003.
- 25 S. L. Barnholtz, J. D. Lydon, G. Huang, M. Venkatesh, C. L. Barnes, A. R. Ketring and S. S. Jurisson, *Inorg. Chem.*, 2001, **40**, 972–976.

- 26 M. Tonelli, S. Turrell, O. Cristini, H. El Hamzaoui, B. Capoen, M. Bouazaoui, C. Kinowski, M. Gazzano and M. C. Cassani, In *Proc. SPIE*; 2012; **8424**, 84242V.
- 27 H. P. Klug and L. E. Alexander, *X-Ray Diffraction Procedures: For Polycrystalline and Amorphous Materials*, Wiley, 1974.
- 28 S. Link and M. A. El-Sayed, *J. Phys. Chem. B*, 1999, **103**, 4212–4217.
- 29 N. Pinçon, B. Palpant, D. Prot, E. Charron and S. Debrus, *Eur. Phys. J.*, 2002, **19**, 395–402.
- 30 L. B. Scaffardi, N. Pellegrini, O. De Sanctis and J. O. Tocho, *Nanotechnology*, 2005, **16**, 158–163.
- 31 C. Worsch, M. Kracker, W. Wisniewski and C. Rüssel, *Thin Solid Films*, 2012, **520**, 4941–4946.
- 32 M. R. Rahman, F. S. Saleh, T. Okajima and T. Ohsaka, *Langmuir*, 2011, **27**, 5126–5135.
- 33 J. Sharma and K. P. Vijayamohanan, *J. Colloid Interface Sci.*, 2006, **298**, 679–684.
- 34 A. Uysal, B. Stripe, B. Lin, M. Meron and P. Dutta, *Phys. Rev. Lett.*, 2011, **107**, 115503.
- 35 A. Fukuoka, H. Araki, J. Kimura, Y. Sakamoto, T. Higuchi, N. Sugimoto, S. Inagaki and M. Ichikawa, *J. Mater. Chem.*, 2004, **14**, 752–756.
- 36 O. Horváth and K. L. Stevenson, *Charge Transfer Photochemistry of Coordination Compounds*, Wiley-VCH, 1993.
- 37 M. L. Marin, K. L. McGilvray and J. C. Scaiano, *J. Am. Chem. Soc.* 2008, **130**, 16572–16584.
- 38 M. Harada, K. Okamoto and M. Terazima, *J. Colloid Interface Sci.*, 2009, **332**, 373–381.
- 39 G. V. Krylova, A. M. Eremenko, N. P. Smirnova and S. Eustis, *Theor. Exp. Chem.*, 2005, **41**, 365–370.
- 40 K. A. Barakat, T. R. Cundari, H. Rabaâ and M. A. Omary, *J. Phys. Chem. B*, 2006, **110**, 14645–14651.
- 41 L. R. Cohen, L. A. Peña, A. J. Seidl, J. M. Olsen, J. Wekselbaum and P. E. Hoggard, *Monatshefte Für Chem.: Chem. Mon.*, 2009, **140**, 1159–1165.

- 42 A. C. Ferrari and J. Robertson, *Phys. Rev. B: Condens. Matter Mater. Phys.*, 2000, **61**, 14095–14107.
- 43 R. Paschotta, *Encyclopedia of Laser Physics and Technology*; Wiley-VCH, 2008.
- 44 F. H. M. Faisal, *Theory of Multiphoton Processes*, Springer, 1987.
- 45 S. C. Chen, C. Y. Tang and Z. D. Yu, *Important Inorganic Chemical Reactions*, Science and Technology Shanghai, 1994.
- 46 K. Chan, B. T. Goh, S. A. Rahman, M. R. Muhamad, C. F. Dee and Z. Aspanut, *Vacuum*, 2012, **86**, 1367–1372.
- 47 A. Serrano, O. R. de la Fuente and M. A. García, *J. Appl. Phys.*, 2010, **108**, 074303.
- 48 B.W. Jacobs, R.J.T. Houk, B.M. Wong, A.A. Talin and M.D. Allendorf, *Nanotechnol.*, 2011, **22**, 375601